Supporting Information

A competitive self-powered sensing platform based on visible light assisted zinc-air battery system

Junlun Zhu[a], Wei Nie[a], Qin Wang[a], Wei Wen[a,*], Xiuhua Zhang[a], Fujun Li[b], Shengfu Wang[a,*]

[a] Hubei Collaborative Innovation Centre for Advanced Organic Chemical Materials & Ministry of Education Key Laboratory for the Synthesis and Application of Organic Functional Molecules, College of Chemistry and Chemical Engineering, Hubei University, Wuhan 430062, People's Republic of China

[b] Key Laboratory of Advanced Energy Materials Chemistry (Ministry of Education), Renewable Energy Conversion and Storage Center (RECAST), College of Chemistry, Nankai University, Tianjin 300071, PR China

*Corresponding author

E-mail address: wangsf@hubu.edu.cn ; wenwei@hubu.edu.cn ;

Experimental Procedures

1 Chemicals and Materials

2,2':5',2''-terthiophene (TTh), 3,3',5,5'-tetramethylbenzidine (TMB), and hydrogen peroxide (H_2O_2) were purchased from Aladdin Reagent Co., Ltd (Shanghai, China). Lithium perchlorate ($LiClO_4$), acetonitrile, glucose, ethanol and other reagents were purchased from Sinopharm Chemical Reagent Co., Ltd (Shanghai, China). All other reagents were analytical grade. Hydrogen tetrachloroaurate (III) trihydrate ($HAuCl_4 \cdot 3H_2O$) and trisodium citrate were obtained from Sigma-Aldrich (USA). Glucose oxidase was obtained from Shanghai Yuanye Biological Co., Ltd (Shanghai, China). The use of ultrapure water (18.25 MΩ•cm) throughout the course of the experiment was from the Aquapro water purification system. Buffer solution was 0.1 M phosphate buffer saline (pH 7.0) which was prepared with Na_2HPO_4 and KH_2PO_4. All solutions were prepared with ultrapure water. Indium tin oxide (10 * 45 * 1 mm) (ITO electrode) was obtained from South China Science & Technology Co., Ltd., Shenzhen, China)

2 Apparatus and Instrumentation

All electrochemical measurements were carried out with a model CHI660E electrochemical analyser (Chenhua Instrumental Co., Ltd, Shanghai, China) at room temperature. The three electrode system consisted of a ITO electrode (10 mm * 10 mm) as the working electrode, saturated calomel electrode (SCE) as the reference electrode, and platinum wire as the counter electrode. Impedance measurements were performed by applying an ac voltage of 10 mV amplitude in the 0.01 to 10^5 Hz frequency range in a 5.0 mM $K_3[Fe(CN)_6]$ / $K_4[Fe(CN)_6]$ redox probe solution with 0.1 M KCl. The open circuit potential signals were carried out by CHI660E electrochemical workstation with a two-electrode system, which pTTh modified ITO electrode as cathode, Zn rod as anode and 20 mW handheld flashlight as light source. The open circuit potential (E^{ocpt}) of Zn-Air cell was measured by the connection of the metal-anode with the photocathode in the electrolytic cell, and 0.1 M PBS (pH=7.0) was used as the supporting electrolyte for open circuit potential (E^{ocpt}) measurements.

The morphology of the pTTh and gold nanoparticles were studied using a FEI-Tecnai G2 transmission electron microscope (TEM) operating at an acceleration voltage of 100 kV. The topographical changes of the ITO electrode surface were performed by SIGMA 500 scanning electron microscope (SEM) which was purchased from ZEISS Ltd., (Germany). Fourier-transform infrared (FT-IR) spectra were measured collected on NICOLET iS10 spectrophotometer (Thermo scientific, USA) using KBr pellets technique in the range of 4000 cm^{-1} to 400 cm^{-1}.Ultraviolet-visible (UV-Vis) absorption spectra were recorded on a UV-Vis spectrophotometer (UV-2700, Shimadzu, Japan). UV-visible diffuse reflectance spectrum was characterized by a Cary 6000i UV-Vis-NIR (Agilent

Technologies Instrument Corporation). Roman spectra were collected on inVia Reflex Confocal micro-Roman spectrophotometer (Renishaw, English). Ultroviolet photoelectron spectrometer (UPS) measurements were carried out on an ESCALAB 250Xi instrument.

3 Preparation of gold nanoparticles

Wine red gold nanoparticles (Au NPs) with average diameter 15 nm were prepared using the citrate reduction method according to the reported[1]. All glassware used in the synthesis have been thoroughly washed in aqua regia (mixture of concentrated hydrochloric acid and concentrated nitric acid in a volume ratio of 3: 1) and rinsed with ultrapure water several times, and oven dried before use. 4.5 mL of 1% trisodium citrate was added dropwise to a 250 mL Erlenmeyer flask containing 100 mL of a 0.01% boiling $HAuCl_4$ aqueous solution. After about one minute, the solution turned dark red. Continue boiling for 10 minutes to stop heating, and then stir the colloidal solution for another 15 minutes. The obtained Au NPs solution was stored in a brown narrow-mouth flask at 4 °C, and its maximum absorption wavelength was 520 nm. The freshly prepared Au NPs solution was used in the next experiment.

4 Preparation of pTTh modified ITO photocathode

The pTTh modified ITO electrode was obtained by cyclic voltammetry (CV) electropolymerization in acetonitrile solution containing 10 mM TTh and 0.10 M $LiClO_4$, the potential range is 0 to 1.2 V, the scan rate is 25 mV s^{-1}, the CV deposition by two cycles. The electrochemical cyclic voltammetry curve was completed by a three-electrode system in which ITO electrode was used as a working electrode, saturated calomel electrode was used as a reference electrode, and platinum electrode was used as an auxiliary electrode. Electrodeposited electrodes were blown dry by nitrogen for further experiments. The prepared electrode is recorded as pTTh / ITO.

5 Fabrication of Gox / Au NPs / pTTh modified ITO electrode

The pTTh / ITO were dipped into 80 μL Au NPs aqueous solution for overnight at room temperature. The prepared electrode is recorded as Au NPs / pTTh / ITO. Au NPs were conjugated onto the pTTh / ITO electrode via classic self-assembly reaction (Au and S) between S elements on the surface of the pTTh and Au from Au NPs. Then, the Au NPs / pTTh / ITO washed with ultrapure water and were immersed freshly prepared 80 μL 0.5 mg mL^{-1} glucose oxidase solution for 3 hours. The prepared electrode is recorded as Gox / Au NPs / pTTh / ITO. The biological connection between Gox and Au NPs is formed by self-assembly of Au-S bonds.

6 Fabrication and measurement of the Zn-air cell sensor

The Zn-air cell sensor was developed by Zn rod as anode and Gox / Au NPs / pTTh / ITO electrode as photocathode. The electrochemical test platform is a self-contained self-powered detection system. For glucose detection, Gox / Au NPs / pTTh / ITO firstly removed the incompletely reacted Gox by rinsing the electrode surface with buffer solution. Then, the Gox / Au NPs / pTTh / ITO

electrode was placed in the cathode chamber containing different concentrations of glucose and O_2 saturated buffer solution for 15 min at 37 ^oC. 15 min later, the open circuit potential (E^{ocpt}) of Gox / Au NPs / pTTh / ITO electrode was measured by CHI660E electrochemical analyser.

Results and Discussion

Valence and conduction band analysis

Band gap calculation by using the following formula:

$$(\alpha h\nu)^2 = A(h\nu - E_g)^{1/2} \quad \textbf{(Equation 1)}^2$$

Where α represents the absorption coefficient, h represents the Planck constant, ν represents the frequency, A represents constant and E_g represents the energy gap for the semiconductor.

As indicated in the **Equation 2**， it is important to understand absolute vacuum scale (E_{AVS}) to calculate the valence band (VB) and conduction band (CB) of normal hydrogen electrode.

$$E(NHE) = - E(_{AVS}) - 4.5 \quad \textbf{(Equation 2)}^3$$

UPS and UV-Vis **DRS spectrum analysis**

The abscissa is the Fermi level (E_F) relative to the gold binding energy, which is defined based on the energy of the electron before excitation relative to the vacuum level. Figure 2A displayed high binding energy cut off ($E_{cut\ off}$) of pTTh film. $E_{cut\ off}$ can be linearly extrapolated to where the yield of secondary electrons is zero to obtain a credible $E_{cut\ off}$, namely $E_{cut\ off}$ is equal to 16.68 eV. The photon energy of the truncated photoelectric signal, 21.2 eV, can only excite electrons with a binding energy of 16.68 eV at most, so that it does not reach the sample surface without any scattering. Figure 2B displayed the HOMO region (0 - 3 eV) for pTTh film. The HOMO energy is determined by using the incident photon energy (hν = 21.2 eV), $E_{cut\ off}$, and the $E_{on\ set}$ (the onset of pTTh film relative to the Fermi energy of gold). By analyzing the data in Figure 2B, the pTTh film of $E_{on\ set}$ is equal to 0.52 eV. E_{HOMO} can be calculated from the **Equation 3**.

$$E_{HOMO} = h\nu - (E_{cut\ off} - E_{on\ set}) \quad \textbf{(Equation 3)}^4$$

The pTTh film of E_{HOMO} is equal to -5.04 eV. The LUMO energy was calculated using the HOMO levels and the optical gaps (E_g) obtained from UV-Vis DRS shown in Figure 2C and 2D. The UV-Vis DRS showed that pTTh has a wide absorption range with an absorption edge of 630 nm. Using the formula to calculate the optical band gap is 1.95 eV. Therefore, the pTTh film of E_{LUMO} is equal to -3.09 eV.

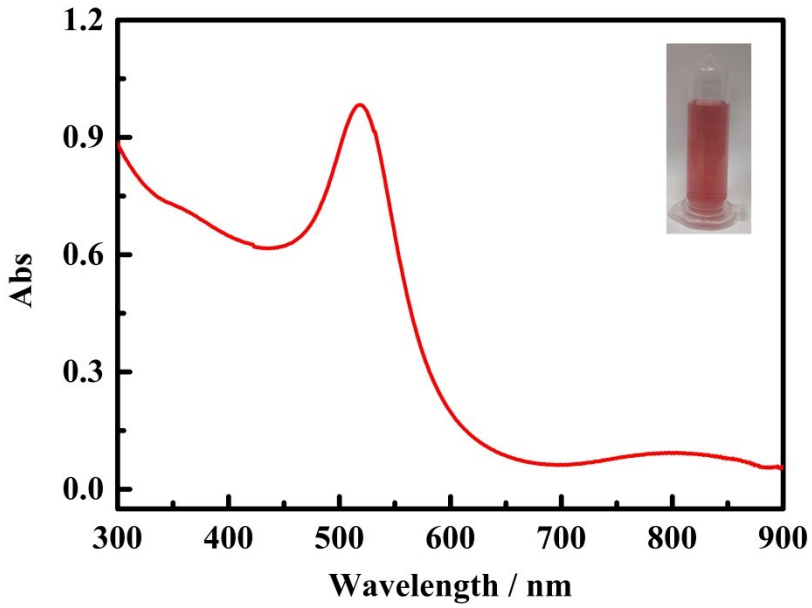

Figure S1 UV-Vis absorption spectrum of Au NPs.

The synthesis of wine-red Au NPs exhibited a strong absorption at 520 nm, in agreement with our group previous report.

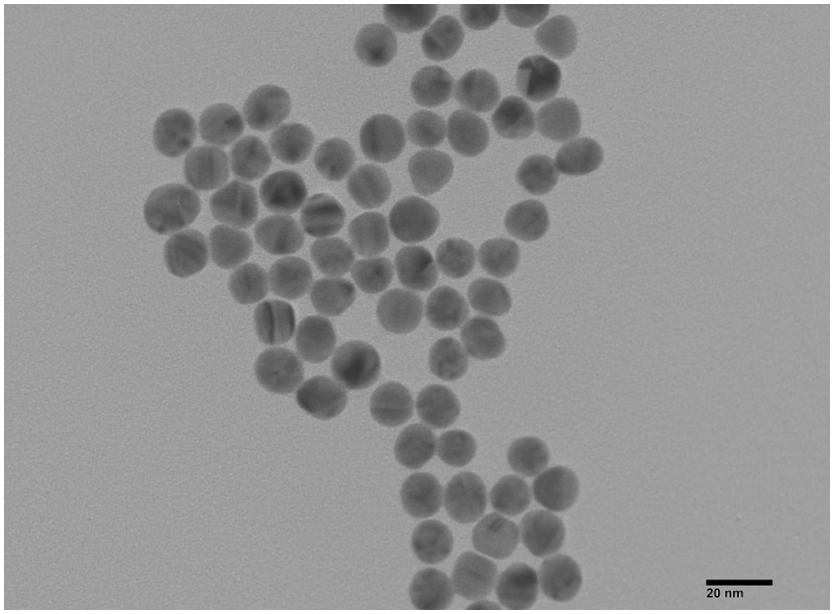

Figure S2 TEM image of Au NPs.

TEM image showed a uniform sphere.

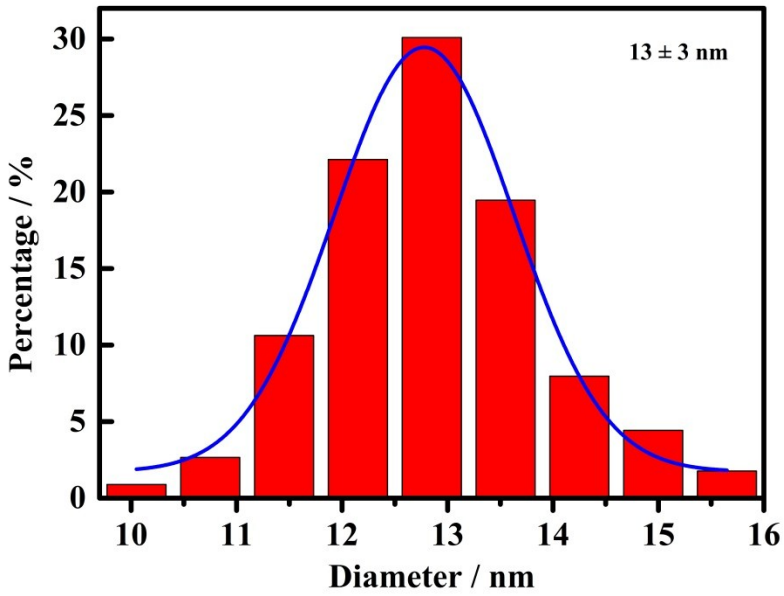

Figure S3 Particle size distribution of Au NPs.

Particle size distribution chart showed a uniform sphere with a particle size of about 13 ± 3 nm

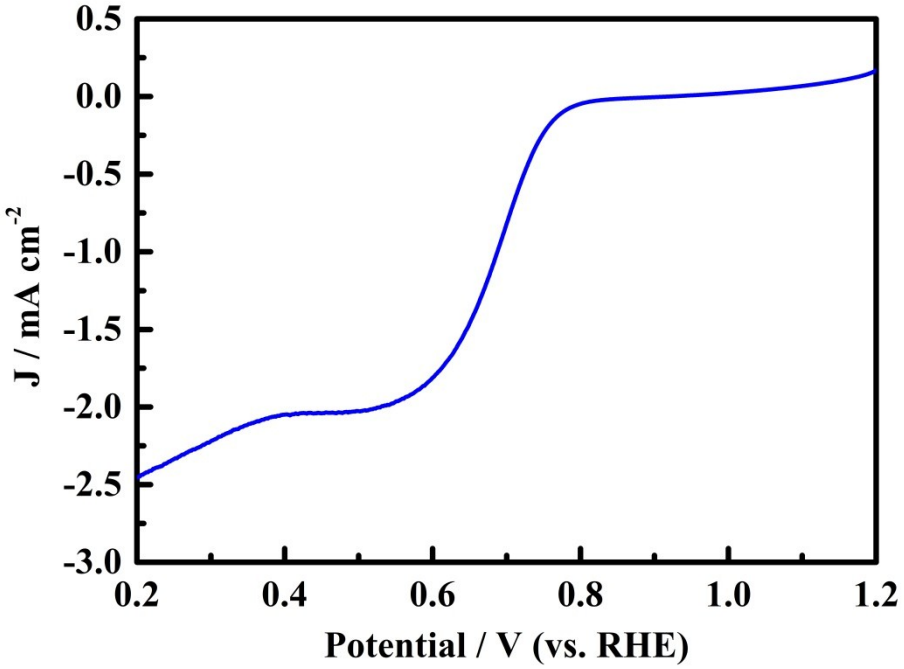

Figure S4 ORR performance of pTTh in 1.0 M KOH solution.

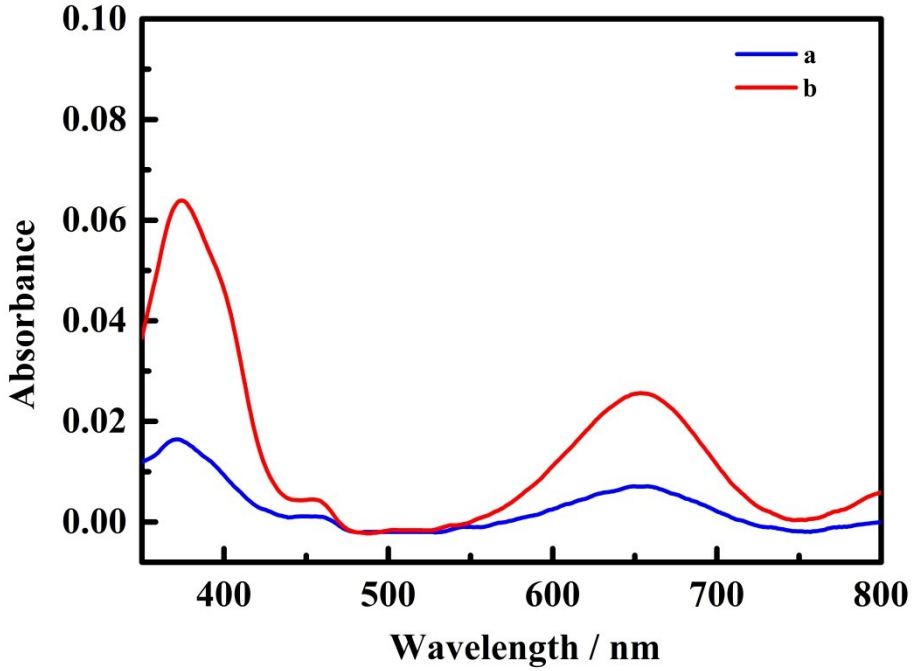

Figure S5 UV-visible absorption spectrum of no light pTTh (blue) solution and light pTTh (red) solution. A total of 3.5 mL of solution, containing 100 μL of 10 mM TMB, 100 μg of horseradish peroxidase, 2 mL of acetate buffer, 1.5 mL of pTTh reaction solution.

Visual resolution of colorimetric hydrogen peroxide (light and no light).

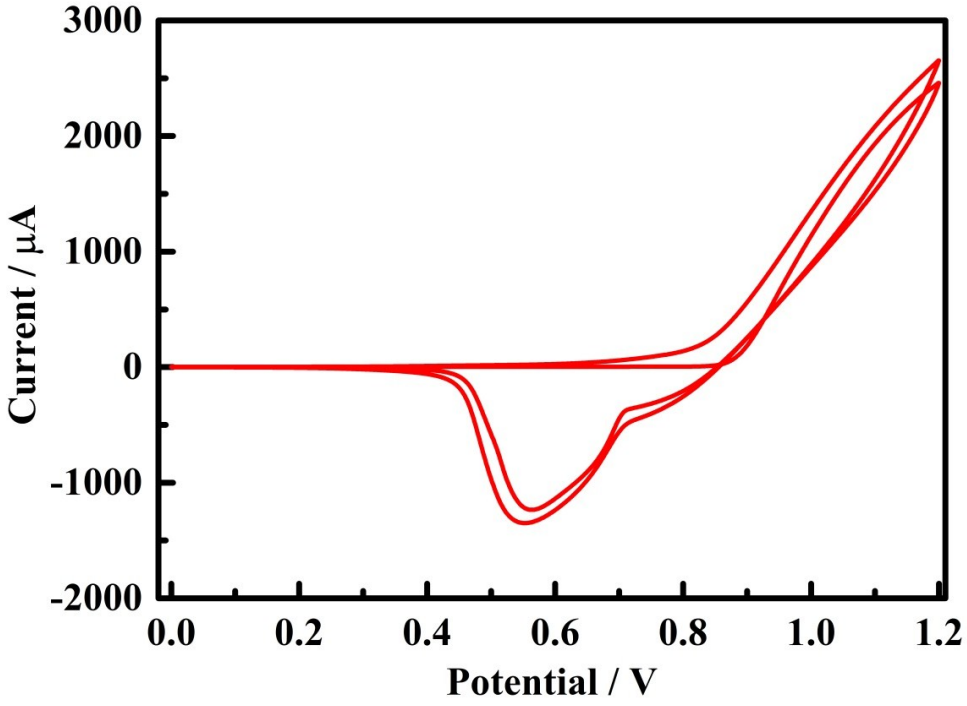

Figure S6 CV electropolymerization of TTh on ITO in acetonitrile solution containing 10 mM TTh and 0.10 M $LiClO_4$ with scan rate of 25 mV s^{-1}.

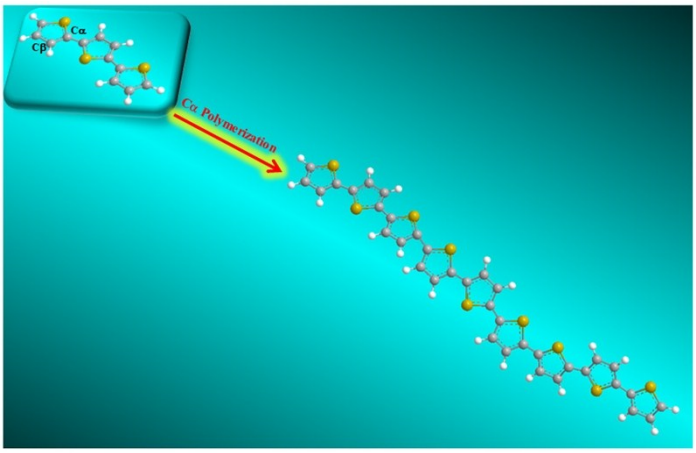

Figure S7 Schematic diagram of TTh electropolymerization to pTTh.

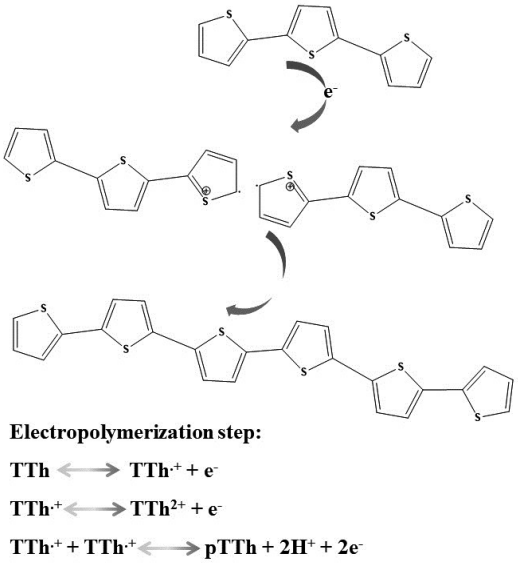

Figure S8 The electropolymerization mechanism of TTh to pTTh.

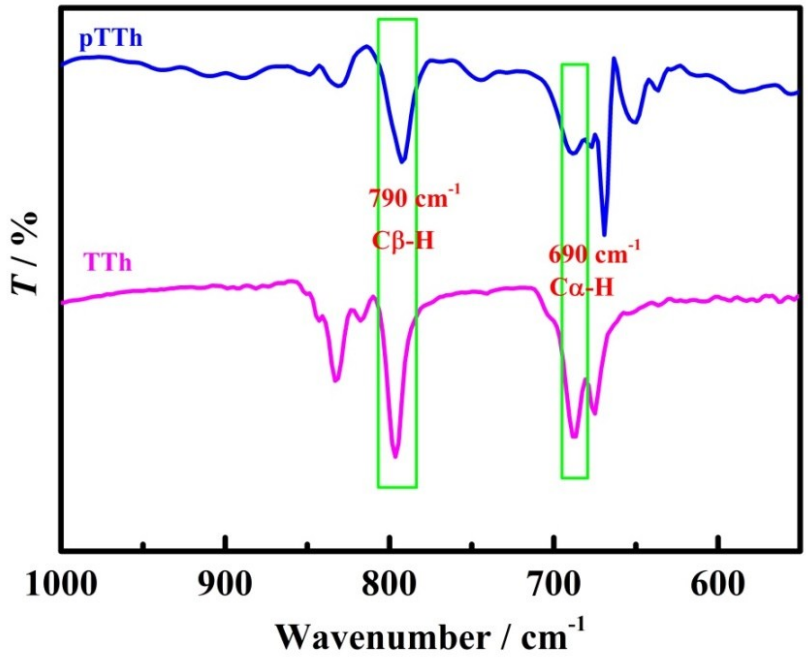

Figure S9 FT-IR spectra of TTh (pink) and pTTh (blue).

The absorption peaks at 690 cm^{-1} and 790 cm^{-1} were attributed to out-of-plane bending vibrations of Cα-H and Cβ-H, respectively. Therefore, the intensity of the absorption peak at 690 cm^{-1} weakened after the polymerization of TTh.

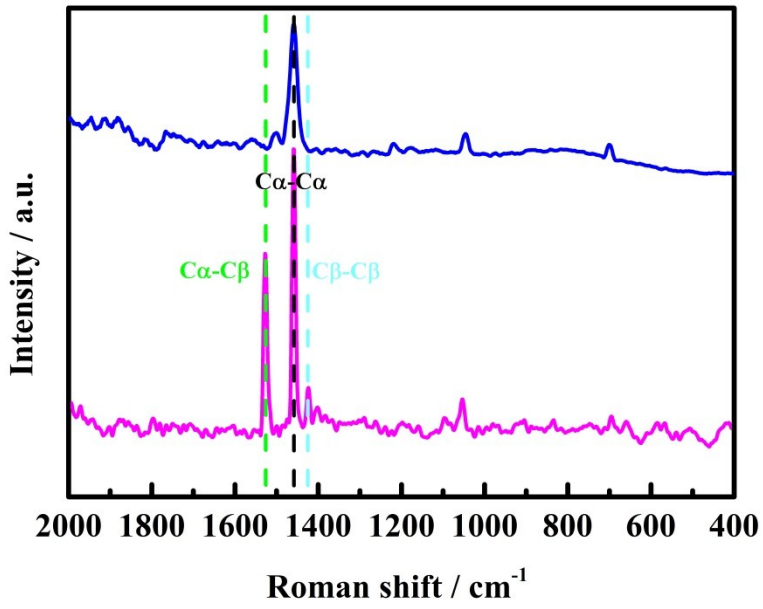

Figure S10 Roman spectra of TTh (pink) and pTTh (blue).

The Raman shift peaks at 1540 cm^{-1}, 1470 cm^{-1}, and 1400 cm^{-1} were attributed to the vibrations of Cα-Cβ, Cα-Cα, and Cβ-Cβ, respectively.

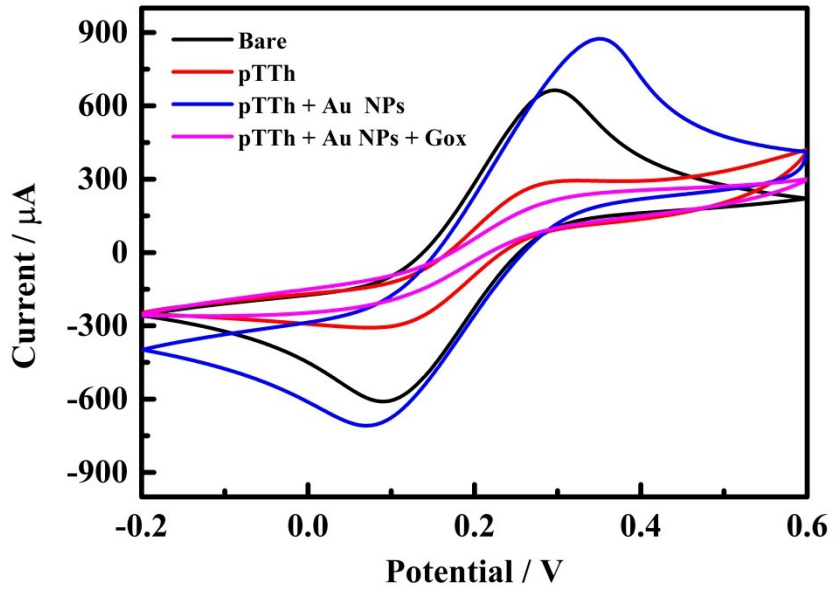

Figure S11 CV spectra of bare ITO (black), pTTh / ITO (red), Au NPs / pTTh / ITO (blue) and Gox / Au NPs / pTTh / ITO (pink).

The CV of bare ITO electrode presented large peak current and a pair of quasi-reversible redox peaks of ($Fe(CN)_6^{3-}$ / $Fe(CN)_6^{4-}$) (curve black). After the TTh solution was electropolymerized into pTTh film on the ITO electrode, an apparent decrease in redox peak current was obtained due to the poor electrical conductivity of pTTh film inhibited electron transfer (curve red). Furthermore, when Au NPs were fixed on the ITO / pTTh film electrode, the good conductivity of Au NPs improves the electron transport ability of ITO / pTTh film electrode, resulting in an increase in the redox peak current (curve blue). After bio-conjugating with the Gox, a slight decrease of the redox peak current appeared (curve pink) due to the poor conductivity of Gox absorbed the ITO / pTTh / Au NPs electrode surface.

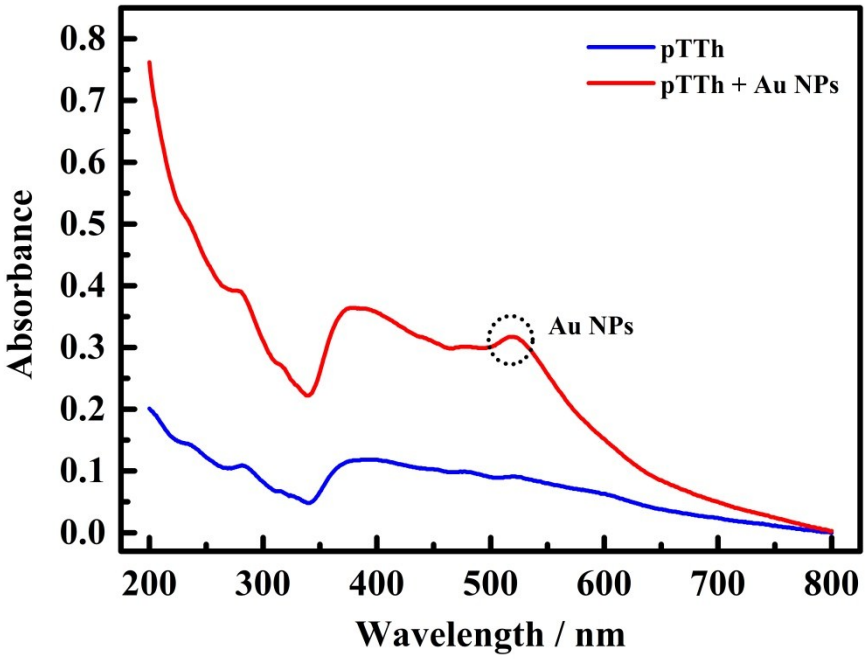

Figure S12 UV-Vis absorption spectroscopy of pTTh solution (blue) and pTTh + Au NPs solution (red).

As shown in **Figure S12**, it can be seen in the UV-Vis absorption chart of pTTh and pTTh composite Au NPs that a clear absorption peak appears at 520 nm, which is attributed to the SPR effect of Au NPs.

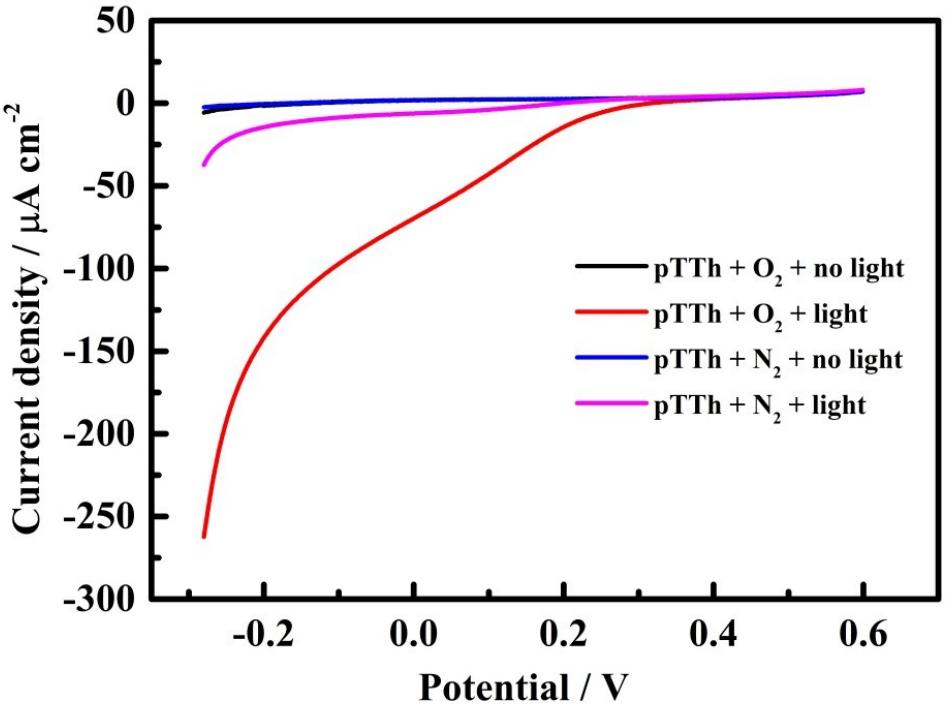

Figure S13. Polarization curves of the photocathode in O_2-saturated electrolyte solution (black curve) without and (red curve) with illumination; N_2-saturated electrolyte solution (blue curve) without and (pink curve) with illumination.

As can be seen from **Figure S13**, under no light conditions (curve black and blue), no catalytic current was obviously exhibited. In the presence of O_2, the pTTh cathode displayed high electrocatalytic activity in O_2-saturated electrolyte under light illumination (curve red). When the oxygen concentration is low, the electrocatalytic activity is very low under light illumination (curve pink).

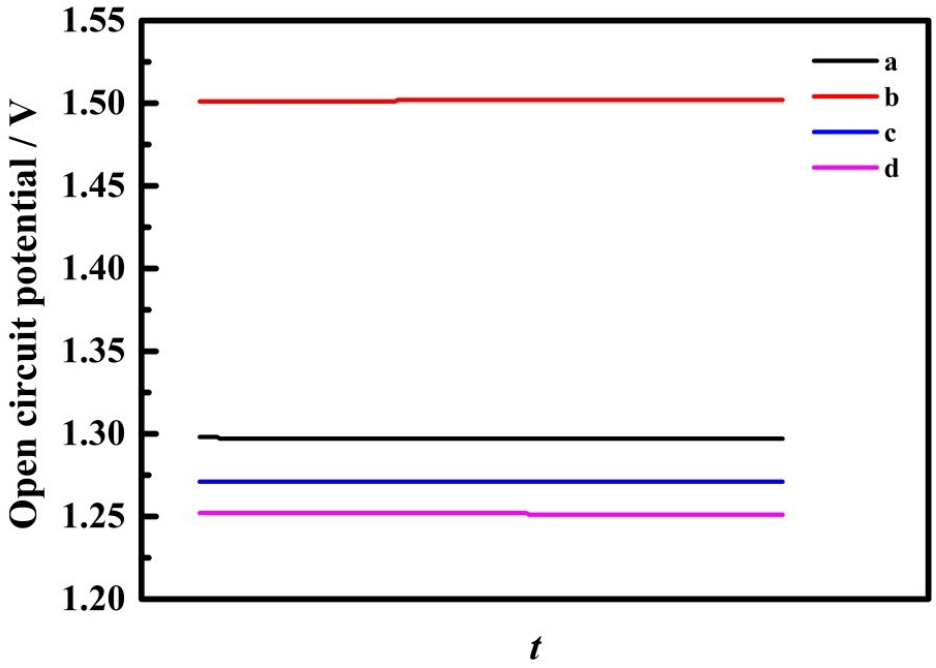

Figure S14. E^{ocpt} response of the pTTh in O_2-saturated and 1 mM H_2O_2 electrolyte solution (black curve) without and (red curve) with illumination; N_2-saturated and 1 mM H_2O_2 electrolyte solution (blue curve) with and (pink curve) without illumination.

To further prove the effect of light illumination, hydrogen peroxide, and oxygen contents, as depicted in **Figure S14**, under light illumination and O_2-saturated electrolyte conditions (curve red), the highest E^{ocpt} was obviously exhibited. When there is no oxygen or light, it has not obvious effect, and hydrogen peroxide does not affect the E^{ocpt}. When there is no oxygen or light, it has not obvious effect, and hydrogen peroxide does not affect the E^{ocpt}. Throughout this process, these results confirmed that hydrogen peroxide has a small effect on the E^{ocpt} response and light and oxygen have a large effect on the E^{ocpt}.

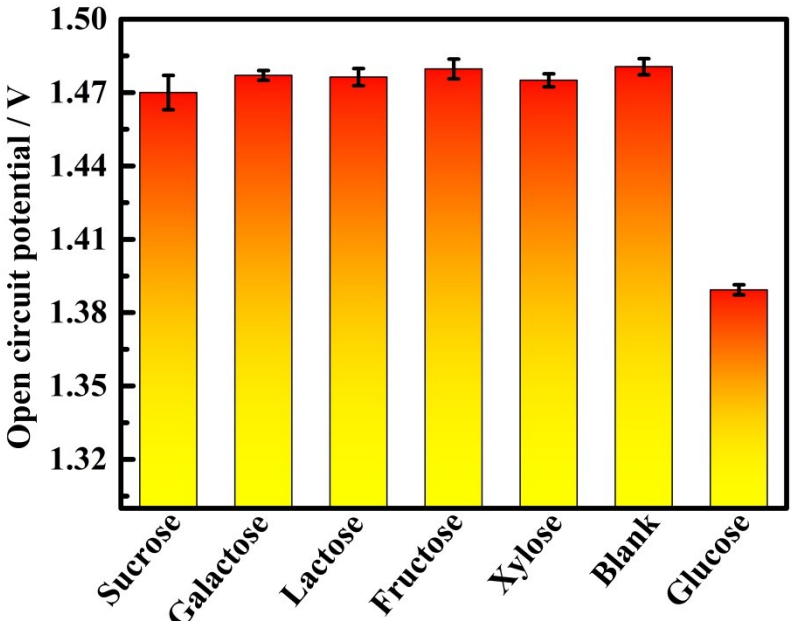

Figure S15. Comparison of E^{ocpt} signal responses with 500 μM different carbohydrates: sucrose, galactose, lactose, fructose, xylose, blank and 10 μM glucose.

Some interfering agents of 500 μM, such as lactose, galactose, sucrose, fructose, and xylose, were used to evaluate the selectivity of the proposed sensor. As described in **Figure S15**, the five interfering carbohydrates displayed negligible E^{ocpt} signal response vary on the proposed SPS compared with the black and added 10 μM glucose, respectively. It expounded that the SPS exhibited a best specificity because of the selective recognizing catalytic reaction between the enzyme specificity and the substrate.

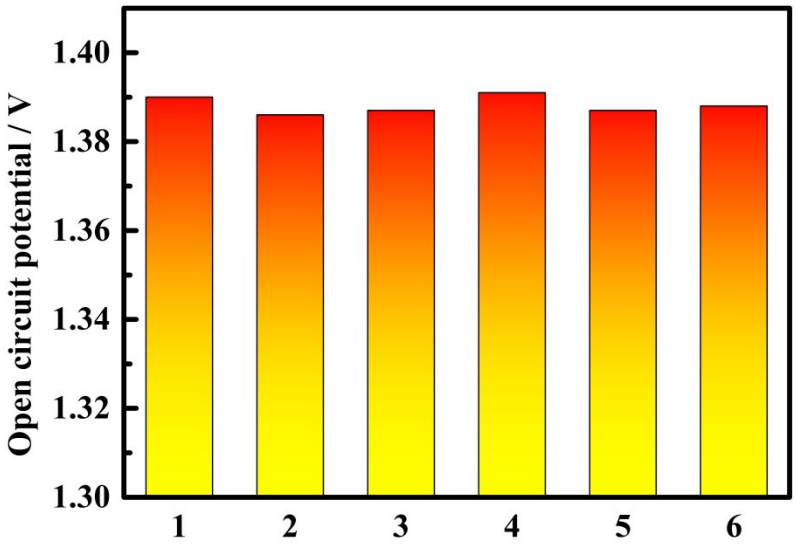

Figure S16. The E^{ocpt} response reproducibility of proposed sensor with different electrode.

The reproducibility of the assay was evaluated by incubating the proposed sensor in glucose, which six independently prepared ITO / pTTh / Au NPs / Gox electrodes for detection glucose. As shown in **Figure S16**, the relative standard deviation of the response for detecting 10 μM glucose were 1.9 %, indicated that the SPS have good reproducibility.

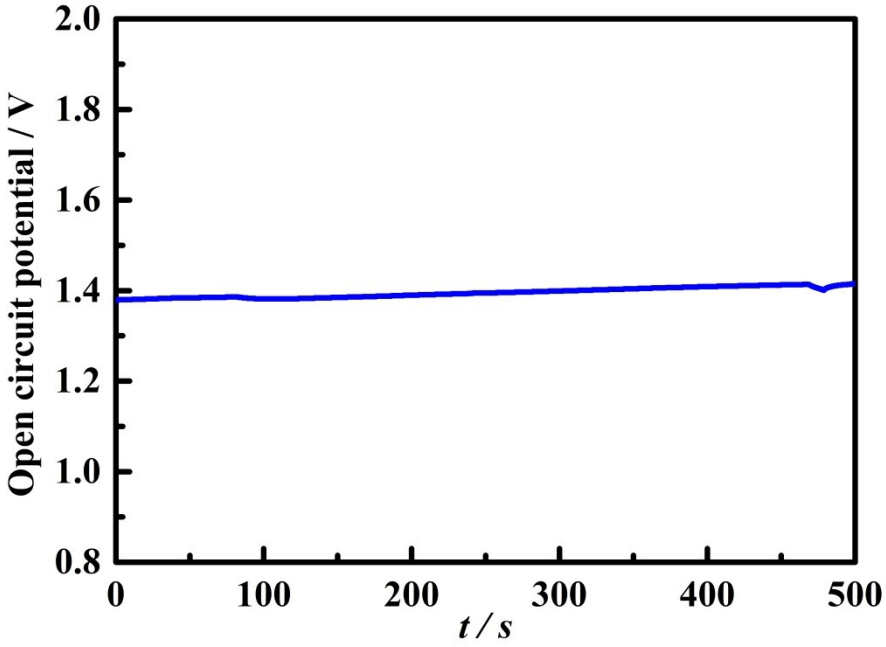

Figure S17 The E^{ocpt} signal response stability of proposed self-powered sensing platform with 10 μM glucose.

The stability of the SPS was assessed in 10 μM glucose (**Figure S17**). The relative standard deviations of 1.2 % in 0 to 600 s suggested a good stability of the sensor, which could be attributed to the excellent E^{ocpt} stability of the SPS based on zinc-air battery system.

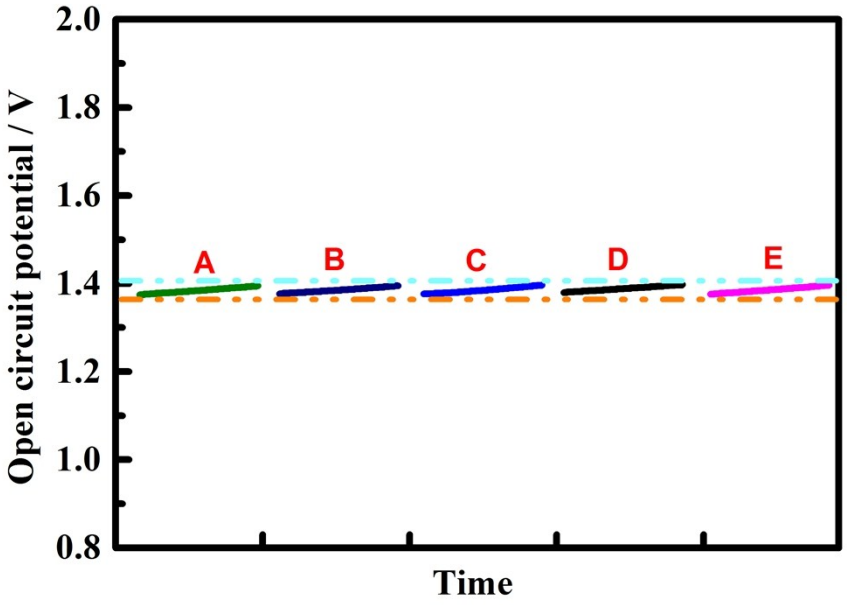

Figure S18 The stability of several times E^{ocpt} signal responses of the proposed self-powered sensing platform with 10 μM glucose.

The stability of several times E^{ocpt} signal responses of the SPS was obtained in 10 μM glucose (Figure S18). This results reveal that the proposed SPS has good stability.

Table S1. The comparison of parameters of different metal-air batteries.[5]

Batteries	Theoretical Voltage (V)	Theoretical specific capacity (Ah Kg^{-1})	Theoretical energy density ($kWh\ kg^{-1}$)
Li-Air	3.4	1170	13.0
Mg-Air	3.1	920	6.8
Al-Air	2.7	1030	8.1
Zn-Air	1.6	658	1.3

Table S2. The proposed sensor was compared with recently reported methods for determination of glucose.

Methods	Linear range[μM]	Detection limit[μM]	Ref
Self-powered photoelectrochemical	1-10000	0.3	6
Electrochemistry	100-10000	#	7
Electrochemistry	0.5-278	0.1	8
Fluorescent	0-200	8.9	9
Colorimetric	1-500	0.487	10
Colorimetric	100-500	30	11
SERS	#	#	12
Electrochemistry	0.1 - 200	0.0737	This work

means not given in related literature.

Table S3: An overview on recently reported self-powered sensors for open circuit potential.

System	Target	Open circuit potential	Reference
Enzymatic biofuel cell	Single nucleotide polymorphisms	0.12 V – 0.3 V	13
Enzymatic biofuel cell	miRNA-141	0.4 V – 0.6 V	14
Enzymatic biofuel cell	miRNA-21	0.4 V – 0.6 V	15
Photoelectrochemical biofuel cell	Circulating tumor cells	0.47 V – 0.51 V	16
Photocatalytic fuel cell	PCB77	0.39 V – 0.41 V	17
Photoassisted-Zn-Air battery	Glucose	1.34 V – 1.47 V	This work

References

1. C. Qin, W. Wen, X. Zhang, H. Gu, S. Wang, *Chem. Comm*. 2015, **51**, 8273-8275.

2. K. Wang, Z. Mo, S. Tang, M. Li, H. Yang, B. Long, Y. Wang, S. Song, Y. Tong, *J. Mater. Chem. A* 2019, **7**, 14129-14135.

3. Y. Xu, M. Schoonen, *American Mineralogist*, 2000, **85**, 543–556.

4. X. Gong, M. Tong, F. Brunetti, J. Seo, Y. Sun, D. Moses, F. Wudl, A. Heeger, Adv. Mater. 2011, **23**, 2272–2277.

5. Y. Liu, Q. Sun, W. Li, K. R. Adair, J. Li, X. Sun, Green Energy & Environment 2017, **2**, 246-277.

6. W. Dai, L. Zhang, W. Zhao, X. Yu, J. Xu, H. Chen, *Anal. Chem.* 2017, **89**, 8070-8078.

7. J. Zhu, X. Peng, W. Nie, Y. Wang, J. Gao, W. Wen, J. Selvaraj, X. Zhang, S. Wang, *Biosens. Bioelectron.*, 2019, **141**, 111450.

8. X. Luo, Z. Zhang, Q. Wan, K. Wu, N. Yang, *Electrochemistry Communications* 2015, **61**, 89-92.

9. B. Liu, Z. Sun, P. Huang, J. Liu, *J. Am. Chem. Soc.* 2015, **137**, 1290−1295

10. W. Xu, L. Jiao, H. Yan, Y. Wu, L. Chen, W. Gu, D. Du, Y. Lin, C. Zhu, *ACS Appl. Mater. Interfaces* 2019, **11**, 22096−22101.

11. J. Xiao, Y. Liu, L. Su, D. Zhao, L. Zhao, X. Zhang, *Anal. Chem.* 2019, **91**, 14803−14807.

12. Y. Hu, H. Cheng, X. Zhao, J. Wu, F. Muhammad, S. Lin, J. He, L. Zhou, C. Zhang, Y. Deng, P. Wang, Z. Zhou, S. Nie, H. Wei, *ACS Nano* 2017, **11**, 5558−5566.

13. C. Gu, X. Kong, X. Liu, P. Gai, F. Li, *Anal. Chem.* 2019, **91**, 8697-8704.

14. T. Zhang, H. Chai, F. Meng, Z. Guo, Y. Jiang, P. Miao, *ACS Appl. Mater. Interfaces* 2018, **10**, 36796−36804.

15. P. Gai, C. Gu, T. Hou, F. Li, *ACS Appl. Mater. Interfaces* 2018, **10**, 9325-9331.

16. C. Gu, T. Hou, S. Zhang, P. Gai, F. Li, *J. Mater. Chem. B* 2019, **7**, 2277-2283.

17. K. Yan, Y. Zhu, W. Ji, F. Chen, J. Zhang, *Anal. Chem.* 2018, **90**, 9662-9666.